Full-zone $\mathbf{k}\cdot\mathbf{p}$ parametrization for III-As materials

G. Mugny*†‡, D. Rideau*, F. Triozon†, Y.-M. Niquet†, C. Kriso*, F.G. Pereira*,
D. Garetto§, C. Tavernier* and C. Delerue‡
* STMicroelectronics, 850 rue J. Monnet, 38926 Crolles, France, Email: denis.rideau@st.com
† CEA, LETI, Minatec Campus, 17 rue des Martyrs, 38054 Grenoble Cedex 9, France
‡ IEMN - Dept. ISEN, UMR CNRS 8520, 41 boulevard Vauban, 59046 Lille Cedex, France
§ Synopsys France, 12 rue Lavoisier, 38330 Montbonnot St Martin, France

***Abstract*—This paper presents a modeling study of III-As materials' band structure obtained with a full-zone 54-band $\mathbf{k}\cdot\mathbf{p}$ model. This model, extending the 30-band model of Refs. [1], [2], accounts for (220) bands and allows a better description of the band structure in the vicinity of the K point [2]. The band gaps and effective masses derived from the band structure are compared with values obtained from other methods, such as the empirical pseudopotential method (EPM) and the tight-binding (TB) approach. Band structures for $In_xGa_{1-x}As$ alloys with different *In* mole fraction x are computed within the virtual crystal approximation.**

I. Introduction

InGaAs alloys are promising candidates for future low power consumption nMOSFET. As diffusion of new materials in CMOS offers new opportunities for numerical investigation, an accurate and efficient full-zone band structure model is needed to study effects like strain [2], confinement in hetero-structures [3], [4] or high-field transport. In previous studies, full-zone 30-band $\mathbf{k}\cdot\mathbf{p}$ models have been parametrized for Si, Ge and alloys [2], but also for GaAs [5], with a view to align with bulk *ab initio* simulations and experimental data (band gaps, effective masses and optical matrix elements). Despite its overall accuracy, the 30-band $\mathbf{k}\cdot\mathbf{p}$ model suffers from some non-physical discontinuities between $K[0, 0.75, 0.75]$ and $U[1, 0.25, 0.25]$ equivalent points. Moreover, no parameters exist for InAs. In this paper, we address these issues by introducing a new 54-band $\mathbf{k}\cdot\mathbf{p}$ model (Section II) and by applying it to InAs, GaAs and their alloys (Section III).

II. 54-band $\mathbf{k}\cdot\mathbf{p}$ model

The 54-band Hamiltonian presented in this paper, extending the 30-band Hamiltonian of Refs. [1], [2], [5], accounts for the 15 states corresponding to free-electron states with wave vectors [000], [111] and [200], as well as the 12 states with wave vector [220] (see Ref. [1]). The 12 extra bands are described in the Hamiltonian by 5 degenerated eigenvalues at the Γ-point and 17 matrix coupling elements (see Table I for definition). No additional spin-orbit terms are added to the standard ones, as they increase the complexity and they are supposed to have a negligible impact. Differently from Si and Ge modeling, additional non-zero matrix elements have to be accounted for in group T_d materials such as InAs and GaAs, due to centrosymmetry breaking. Four extra imaginary coupling parameters ($S, S^{'}, U$ and $U^{'}$ in Table I) and one extra SO term ($\Delta_{\Gamma_{15}\Gamma_{25'l}}$) are thus added to the standard 30-band Hamiltonian used for Si.

The Si band structure obtained with parameters given in Table I is shown in Fig.1 and compared to the one obtained

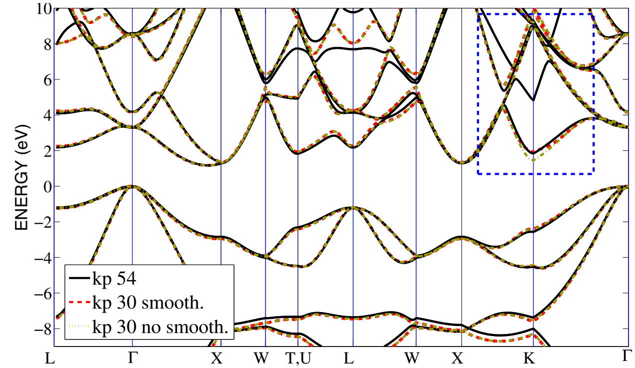

Fig. 1: Bulk Si electronic band structure using 54-band $\mathbf{k}\cdot\mathbf{p}$ model, compared to band structure using 30-band $\mathbf{k}\cdot\mathbf{p}$ model with and without use of smoothing function (see Fig.1 of Ref. [2]). Dashed-line rectangle points out the (220) band effect in the near-K-region.

with 30-band model (Fig.1 of Ref. [2]). One clearly notes the presence of the (220) band as low as 5eV above the valence band maximum in the vicinity of the K point, which was missing in the 30-band model in Ref. [2]. Moreover, without smoothing function the 30-band model predicts a conduction band edge in K that is too low, which is the reason why authors of Ref. [2] introduced a non-physical interpolation of the parameters. Such pragmatic approach is not needed with the 54 $\mathbf{k}\cdot\mathbf{p}$ model, which allows a better description of the near-K-point region, without increasing too much the computational effort of the modeling. The computational complexity for the solution of a complete bulk band structure problem is for both $\mathbf{k}\cdot\mathbf{p}$ models approximately two orders of magnitude lower than the one needed by non-local empirical pseudo-potential methods (EPM).

III. GaAs and InAs band structure

We present new parametrizations for GaAs and InAs with bulk 30- and 54-band $\mathbf{k}\cdot\mathbf{p}$ models in Table I. Two separate optimized parameters sets for 30- and 54-band are presented and we did not use an explicit Löwdin renormalization [6].

A. Methodology for parameters extraction

To extract parameters for III-As, we initially performed empirical pseudo-potential (EPM) calculations with non-local (NL) effects and spin-orbit coupling based on parameters of

978-1-4673-7860-4/15/$31.00 ©2015 IEEE

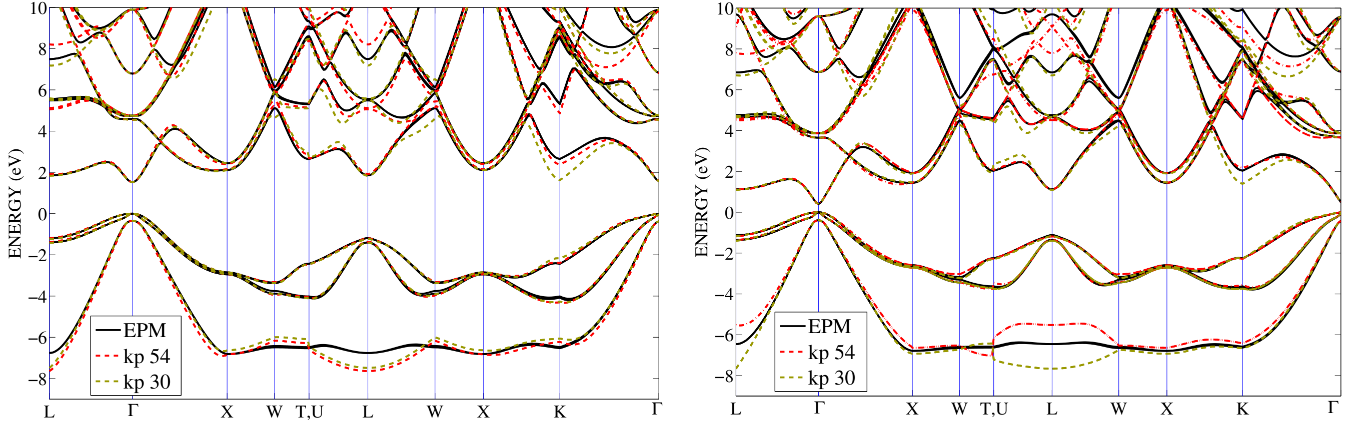

Fig. 2: Bulk electronic band structure for GaAs (left) and InAs (right) using 30-band, 54-band $\mathbf{k}\cdot\mathbf{p}$ and EPM models.

Ref. [7] for GaAs and Ref. [8] for InAs. The extracted band gaps are shown in Table II and a difference with experimental values of less than 40 meV for all relevant gaps is obtained for GaAs. For InAs, we chose parametrization of Ref. [8], as it provides more accurate direct band gap at Γ. However, as will be discussed later, band gaps at X and L symmetry points are more controversial. Effective masses are also extracted by fitting the parabolic dispersion close to band extrema and shown in Table II. While the effective mass in Γ is overestimated for GaAs (which is also the case in previous studies with EPM), all other masses lie within the experimental range of values.

A non-linear optimization algorithm using Nelder-Mead method is then used to find the sets of $\mathbf{k}\cdot\mathbf{p}$ parameters that minimize the least-square error function between $\mathbf{k}\cdot\mathbf{p}$ and EPM eigenvalues on a complex and dense path throughout the Brillouin zone. We tried to match as closely as possible the experimental values for known eigenvalues and effective masses, but some inaccuracy can remain over 10eV and below -6eV.

B. Results for binary alloys

Band structures obtained for GaAs and InAs are shown in Fig. 2 and corresponding $\mathbf{k}\cdot\mathbf{p}$ parameters are given in Table I. Good agreement is found with NL EPM band structures in the energy range considered, especially for the Γ, Δ and L conduction valleys involved in electronic transport. Note that the 54-band $\mathbf{k}\cdot\mathbf{p}$ model allows a better description of the band structure in the near-K-point region, especially for the band minimum in K which is too low in the 30-band $\mathbf{k}\cdot\mathbf{p}$ model. The discontinuity at the T, U transition is also removed for conduction bands, as seen in Fig.2b, but it remains in the valence band below -5eV, where it has no influence on transport.

The band gaps and effective masses extracted from these parametrizations are shown in Table II. Accuracy of the present $\mathbf{k}\cdot\mathbf{p}$ model depends on the reference model chosen, on which parameters have been fitted. For GaAs, the two available EPM parametrizations [7], [8] provide close values for band gaps. For InAs, the values of E_X obtained with the two EPM

TABLE I: Non-zero matrix terms of the momentum $\mathbf{p}$ and their definitions for InAs and GaAs for 54- and 30-band $\mathbf{k}\cdot\mathbf{p}$ models. Letter e indexes the 12 (220) bands. Same convention as Ref. [2] is used for the notations.

Parameter [-]	GaAs	InAs	Si	GaAs	InAs
		54-band		30-band	
$P = \frac{\hbar}{m}\langle\Gamma_{25'l}\vert\hat{p}\vert\Gamma_{2'l}\rangle$	1.2239	1.1170	1.2180	1.1407	1.1284
$Q = \frac{\hbar}{m}\langle\Gamma_{25'l}\vert\hat{p}\vert\Gamma_{15}\rangle$	1.1302	1.0340	1.0430	1.1367	1.0803
$R = \frac{\hbar}{m}\langle\Gamma_{25'l}\vert\hat{p}\vert\Gamma_{12'}\rangle$	0.5580	0.5985	0.5380	0.5887	0.5555
$P' = \frac{\hbar}{m}\langle\Gamma_{25'l}\vert\hat{p}\vert\Gamma_{2'u}\rangle$	0.2207	0.0820	-0.0159	0.1988	0.2718
$P'' = \frac{\hbar}{m}\langle\Gamma_{25'u}\vert\hat{p}\vert\Gamma_{2'l}\rangle$	0.1801	0.1477	0.1535	0.1237	0.2164
$Q' = \frac{\hbar}{m}\langle\Gamma_{25'u}\vert\hat{p}\vert\Gamma_{15}\rangle$	-0.5826	-0.6817	-0.6503	-0.6089	-0.5001
$R' = \frac{\hbar}{m}\langle\Gamma_{25'u}\vert\hat{p}\vert\Gamma_{12'}\rangle$	0.8852	0.7850	0.8598	0.8042	0.8527
$P''' = \frac{\hbar}{m}\langle\Gamma_{25'u}\vert\hat{p}\vert\Gamma_{2'u}\rangle$	1.1860	1.0848	1.4852	1.3913	1.3246
$T = \frac{\hbar}{m}\langle\Gamma_{1u}\vert\hat{p}\vert\Gamma_{15}\rangle$	1.0250	1.1266	1.1637	1.0320	1.0758
$T' = \frac{\hbar}{m}\langle\Gamma_{1l}\vert\hat{p}\vert\Gamma_{15}\rangle$	0.3702	-0.4449	0.2520	0.1991	0.3536
$S = \frac{\hbar}{m}\langle\Gamma_{15}\vert\hat{p}\vert\Gamma_{2'l}\rangle$	-0.0008	-0.0421	–	-0.0013	-0.0408
$S' = \frac{\hbar}{m}\langle\Gamma_{15}\vert\hat{p}\vert\Gamma_{2'u}\rangle$	-0.0031	-0.0679	–	-0.0025	0.1681
$U = \frac{\hbar}{m}\langle\Gamma_{1u}\vert\hat{p}\vert\Gamma_{25'l}\rangle$	0.3373	0.3630	–	0.3209	0.3272
$U' = \frac{\hbar}{m}\langle\Gamma_{1u}\vert\hat{p}\vert\Gamma_{25'u}\rangle$	-0.1185	0.0385	–	-0.1112	0.0430
$A_e = \frac{\hbar}{m}\langle\Gamma_{25e}\vert\hat{p}\vert\Gamma_{25'e}\rangle$	2.0852	2.2635	1.4990		
$Y_e = \frac{\hbar}{m}\langle\Gamma_{12e}\vert\hat{p}\vert\Gamma_{25e}\rangle$	1.0642	1.1634	0.9606		
$Z_e = \frac{\hbar}{m}\langle\Gamma_{12e}\vert\hat{p}\vert\Gamma_{15e}\rangle$	0.0026	0.0318	0.0025		
$T_e = \frac{\hbar}{m}\langle\Gamma_{1e}\vert\hat{p}\vert\Gamma_{15e}\rangle$	2.4442	1.0322	2.9834		
$Q_e''' = \frac{\hbar}{m}\langle\Gamma_{15e}\vert\hat{p}\vert\Gamma_{25'e}\rangle$	1.3565	0.2262	1.6829		
$A_e' = \frac{\hbar}{m}\langle\Gamma_{25e}\vert\hat{p}\vert\Gamma_{25'u}\rangle$	-0.1138	-0.0718	-0.1579		
$A_e'' = \frac{\hbar}{m}\langle\Gamma_{25e}\vert\hat{p}\vert\Gamma_{25'l}\rangle$	0.2324	0.0273	0.2896		
$P_e = \frac{\hbar}{m}\langle\Gamma_{25'e}\vert\hat{p}\vert\Gamma_{2'u}\rangle$	0.0005	0.0004	0.0299		
$P_e' = \frac{\hbar}{m}\langle\Gamma_{25'e}\vert\hat{p}\vert\Gamma_{2'l}\rangle$	-0.2105	-0.0110	-0.3530		
$Q_e = \frac{\hbar}{m}\langle\Gamma_{25'e}\vert\hat{p}\vert\Gamma_{15}\rangle$	0.0100	0.0050	0.1703		
$Q_e' = \frac{\hbar}{m}\langle\Gamma_{15e}\vert\hat{p}\vert\Gamma_{25'u}\rangle$	0.1530	0.0690	0.1258		
$Q_e'' = \frac{\hbar}{m}\langle\Gamma_{15e}\vert\hat{p}\vert\Gamma_{25'l}\rangle$	0.0872	0.0597	0.0066		
$R_e = \frac{\hbar}{m}\langle\Gamma_{12}\vert\hat{p}\vert\Gamma_{25'e}\rangle$	-0.0015	-0.0007	-0.0013		
$T_e' = \frac{\hbar}{m}\langle\Gamma_{15e}\vert\hat{p}\vert\Gamma_{1u}\rangle$	-0.0172	-0.1156	-0.0503		
$T_e'' = \frac{\hbar}{m}\langle\Gamma_{15e}\vert\hat{p}\vert\Gamma_{1l}\rangle$	-0.1808	-0.1045	-0.3486		
$T_e''' = \frac{\hbar}{m}\langle\Gamma_{15}\vert\hat{p}\vert\Gamma_{1e}\rangle$	-0.0007	-0.0234	-0.0267		
$Z_e' = \frac{\hbar}{m}\langle\Gamma_{12e}\vert\hat{p}\vert\Gamma_{15}\rangle$	0.0058	0.0020	0.0054		

TABLE II: Band gaps (with respect to valence band maximum in Γ), spin-orbit and effective masses calculated for GaAs and InAs at T = 0 K. All energies are expressed in eV and masses in unit of m_0. Values in parentheses are calculated with 30-band $\mathbf{k}\cdot\mathbf{p}$. Both EPM values come from our own calculations, with parameters from Refs. [7], [8] and slightly different SO parameters. Experimental values are taken from Refs. [10], except when mentioned.

	GaAs						InAs					
E_g	Exp.	HSE [9]	TB	EPM [8]	EPM [7]	$\mathbf{k}\cdot\mathbf{p}$	Exp.	HSE [9]	TB	EPM [8]	EPM [7]	$\mathbf{k}\cdot\mathbf{p}$
E_Γ	1.519	1.52	1.519	1.518	1.527	1.527 (1.527)	0.42	0.42	0.418	0.405	0.389	0.415 (0.405)
$\Delta_{SO}^{(\Gamma)}$	0.341		0.340	0.340	0.350	0.349 (0.349)	0.39		0.380	0.389	0.440	0.390 (0.390)
E_L	1.85[1]	1.86	1.837	1.812	1.855	1.942 (1.835)	N/A	1.53	1.691	1.122	1.515	1.128 (1.098)
E_X	2.18[1]	2.15	1.989	2.003	2.115	2.162 (2.118)	1.90[2]	1.98	2.176	1.442	2.274	1.456 (1.459)
E_Δ	N/A		1.989		2.088	2.109 (2.058)				–		
$m_e^{*(\Gamma)}$	0.067	0.067	0.067	0.082	0.083	0.074 (0.084)	0.026	0.027	0.023	0.026		0.028 (0.027)
$m_{e,l}^{*(L)}$	1.9		1.44	1.61	1.85	1.41 (1.91)	0.64, 3.57[3]		2.16	1.68	1.76	1.25 (1.43)
$m_{e,t}^{*(L)}$	0.08		0.12	0.13	0.12	0.13 (0.14)	0.05, 0.12[3]		0.11	0.10	0.10	0.11 (0.12)
$m_{e,l}^{*(\Delta)}$	1.30		1.25	1.71	1.45	1.29 (1.17)	1.13, 1.98[3]		1.69	2.31		0.82 (1.55)
$m_{e,t}^{*(\Delta)}$	0.23		0.24	0.24	0.24	0.23 (0.23)	0.16, 0.28[3]		0.28	0.19		0.21 (0.22)
$m_{hh}^{*(001)}$	0.35	0.314	0.33			0.36 (0.36)	0.34 – 0.39	0.34	0.32			0.31 (0.31)
$m_{hh}^{*(110)}$	0.64		0.65			0.68 (0.65)	0.58 – 0.98		0.65			0.58 (0.58)
$m_{hh}^{*(111)}$	0.89		0.92			0.90 (0.84)	0.63 – 0.76		0.96			0.81 (0.80)
$m_{lh}^{*(001)}$	0.090	0.085	0.086			0.098 (0.109)	0.027 – 0.042	0.033	0.029			0.033 (0.033)
$m_{lh}^{*(110)}$	0.081		0.076			0.087 (0.096)	0.026 – 0.041		0.027			0.031 (0.032)
$m_{lh}^{*(111)}$	0.078		0.073			0.084 (0.093)	0.014 – 0.026		0.028			0.031 (0.031)
m_{so}	0.165	0.166	0.161			0.198	0.09 – 0.15	0.112	0.095			0.106 (0.107)

[1] Ref. [11]
[2] Ref. [12]
[3] Ref. [8] and references herein.

parametrizations of Refs. [7] and [8] are 1.4 and 2.1eV respectively (see Fig. 3), while the exhaustive *ab initio* calculations of Ref. [9] reports E_X ranging from 1.65 to 2.09eV. The only experimental value available to our knowledge for E_X is 1.9eV [12]. These results are also compared in Table II and Fig. 3 to those obtained in the $sp^3d^5s^*$ tight-binding model with the parameters from Ref. [13], obtained to fit experimental values at 0K. An overall good agreement is observed for both GaAs and InAs principal band gaps, except for InAs E_X and E_L band gaps, as seen in Fig. 3.

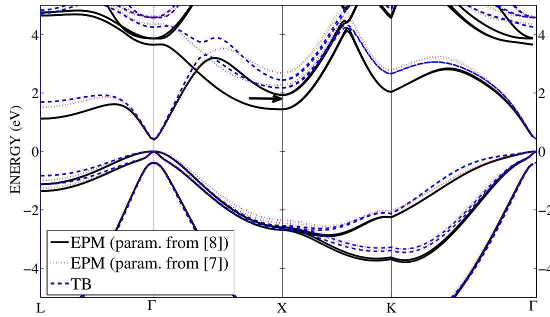

Fig. 3: InAs band structure obtained with our own calculation based on the two NL EPM parametrization of Ref. [7] and [8], and with TB parametrization of Ref. [13]. The experimental value of Ref. [12] for E_X is shown with the black arrow. The EPM models exhibit a net difference, illustrating the controversy on the position of satellite valleys.

C. Density-of-states

The Density-Of-States (DOS) has been computed by integrating the band structure over the Brillouin zone with Gilat and Raubenheimer method [14]. The DOS obtained for GaAs and InAs with our 54-band model is shown on Fig. 4 and compared to the one obtained with NL EPM of Refs. [7] and [15] and our own calculation. As discussed in previous section, the two EPM parametrizations for InAs give different values for indirect band gaps. This discrepancy is visible in Fig. 4b, where the first peak in conduction band is shifted by ∼0.5eV. A zoom of the conduction band edge shows the very low DOS of the Γ conduction valley and the abrupt change of DOS when satellite valleys are reached (around 1.85 eV for GaAs and 1.1eV for InAs). Although InAs has a lower DOS in the Γ conduction band, this abrupt transition is less pronounced. This can be due to its higher non-parabolicity and lower DOS masses of the satellite valleys.

D. Results for $In_xGa_{1-x}As$ alloy

Virtual Crystal Approximation (VCA) has been used to compute $In_xGa_{1-x}As$ band structures for any *In* mole fraction x. In this approximation, a virtual binary crystal is constructed, with atomic parameters interpolated between the two initial elements (*In* and *Ga* atoms in our case). Linear interpolation is made for all parameters, except for the energies $E_g = (\Gamma_{12} - \Gamma^l_{25'})$ and Δ_{SO} for which bowing coefficients B are used:

$$P_{InGaAs} = P_{InAs}x + P_{GaAs}(1-x) - Bx(1-x) \qquad (1)$$

We use values suggested by Ref. [10] which are $B = 0.477$ for E_g and $B = 0.15$ for Δ_{SO}. Although the above reference

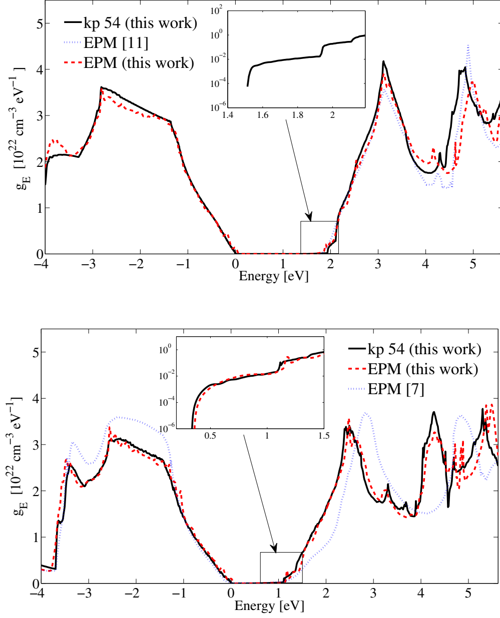

Fig. 4: Density-of-states in GaAs (up) and InAs (down) obtained with our 54-band $\mathbf{k}\cdot\mathbf{p}$ model and compared to EPM results in Refs. [7], [15]. Inset shows a zoom of the conduction band edge in log scale, emphasizing the low DOS of the Γ conduction valley.

suggests to use a bowing coefficient for P parameter in 8-band $\mathbf{k}\cdot\mathbf{p}$ model, an adequate tendency for the band gaps and effective mass $m_e^*(\Gamma)$ is obtained without bowing with our 54-band model, as shown in Fig.5. Fitting back the band gaps $E_L(x)$ and $E_X(x)$ with Eq.1 gives bowing coefficients of 0.72 and 1 respectively, which are in the range of values suggested by Ref. [10]. The difference with experimental results for $m_e^*(\Gamma)$ can be due to temperature influence, as measurement were done at 300K.
For 30-band $\mathbf{k}\cdot\mathbf{p}$ model, additional bowing coefficients had to be introduced on parameters P''', Q' and S ($B = 0.78, 0.2$ and 0.2, respectively) in order to have a correct bowing for band gaps. However no bowing coefficient for P parameter was needed, which is the main parameter influencing $m_e^*(\Gamma)$. The band gaps and effective masses are shown on Fig.6, together with the EPM results from Ref. [8]. One notes that the tendency is very close to the EPM results, especially for $m_e^*(\Gamma)$, which validates the parameter extraction procedure.

IV. Conclusion

New sets of $\mathbf{k}\cdot\mathbf{p}$ parameters have been extracted for modeling the band structure of InAs and GaAs materials. The present model and parameters can be used to study transport in III-As based devices with accurate full-zone band structure. $In_xGa_{1-x}As$ alloy band structures have been computed within the VCA and it was found that without any additional fitting parameter (in the case of 54-band model), the overall tendency is close to previous results obtained with EPM and agrees with the expected analytic relation for main band gaps and effective masses.

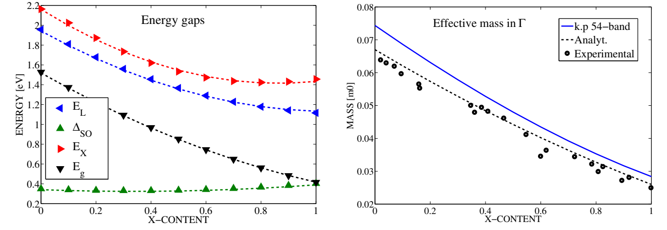

Fig. 5: Band gaps (left) and effective masses (right) bowing as function of *In* mole fraction x for 54-band $\mathbf{k}\cdot\mathbf{p}$ model. Dashed lines show the fits with Eq.1. Experimental values for masses are taken from Ref. [8].

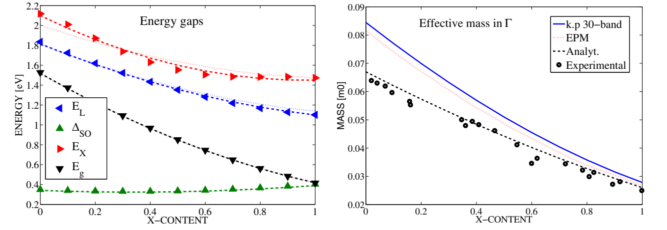

Fig. 6: Band gaps (left) and effective masses (right) bowing as function of *In* mole fraction x for 30-band $\mathbf{k}\cdot\mathbf{p}$ (solid line) and EPM (dotted line). Dashed lines show the fits with Eq.1 (overlying the EPM curve for E_g and Δ_{SO}). Experimental values for masses are taken from Ref. [8].

Acknowledgment

This work was supported by the research project NOODLES ANR-13-NANO-0009 and the research project COMPOSE3 number 619325. The authors also thank Benoît Sklénard at CEA-LETI for fruitful discussions.

References

[1] F. H. Pollak and M. Cardona, *Physical Review*, vol. 172, p. 816, 1968.
[2] D. Rideau *et al.*, *Physical Review B*, vol. 74, p. 195208, 2006.
[3] ——, *Solid-State Electronics*, vol. 53, pp. 452–461, 2009.
[4] S. Boyer-Richard *et al.*, *Applied Physics Letters*, vol. 98, p. 251913, 2011.
[5] S. Richard *et al*, *Physical Review B*, vol. 70, p. 235204, 2004.
[6] P.-O. Löwdin, *The Journal of Chemical Physics*, vol. 19, p. 1396, 1951.
[7] J. R. Chelikowsky and M. L. Cohen, *Physical Review B*, vol. 14, p. 556, 1976.
[8] J. Kim and M. V. Fischetti, *Journal of Applied Physics*, vol. 108, p. 013710, 2010.
[9] Y.-S. Kim *et al.*, *Physical Review B*, vol. 82, no. 20, p. 205212, 2010.
[10] I. Vurgaftman *et al.*, *Journal of applied physics*, vol. 89, p. 5815, 2001.
[11] T.-C. Chiang *et al.*, *Physical Review B*, vol. 21, no. 8, p. 3513, 1980.
[12] W. Drube *et al.*, *Physical Review B*, vol. 35, no. 11, p. 5563, 1987.
[13] J.-M. Jancu *et al.*, *Physical Review B*, vol. 57, no. 11, p. 6493, 1998.
[14] G. Gilat and L. Raubenheimer, *Physical Review*, vol. 144, no. 2, p. 390, 1966.
[15] M. V. Fischetti and S. E. Laux, *Physical Review B*, vol. 38, no. 14, p. 9721, 1988.